Investigation of Ion-Conducting Ormolytes: Structure-Property Relationships

P. Judeinstein,*,†,§ J. Titman,‡ M. Stamm,‡ and H. Schmidt†

Institut für Neue Materialen, Universität des Saarlandes, Geb. 43, D-6600 Saarbrücken, Germany, and Max-Planck-Institut für Polymerforschung, Ackermannweg 10, Postfach 3148, D-6500 Mainz, Germany

Received August 5, 1993. Revised Manuscript Received November 22, 1993®

Hybrid organic-inorganic composites with ionic properties, so called ormolytes (organically modified electrolytes) have been prepared by the sol-gel process from mixtures of tetraethoxysilane, tetraethylene glycol, and lithium salt. They show ionic conductivity up to 5×10^{-5} Ω^{-1} cm^{-1}, with activation energies around 0.6 eV. Their properties have been related to their structure using a multitechnique approach (IR, DSC, NMR, SAXS). These materials can be described as diphasic systems with silica clusters providing the mechanical properties and the organic phase allowing the dissolution of large quantities of salts. Optical transparency and mechanical stability can be explained by the interpenetration of these two phases at a molecular level.

Introduction

Over the past few years, there have been a great deal of studies in the field of solid electrolytes.[1] These materials are of great interest for various applications such as batteries, energy and data storage, sensors, electrochromic, and photoelectrochemical devices.[2] Systems based on conductivity induced by the addition of lithium appear to offer the most favorable properties.[3] The most promising materials involve lithium salts dissolved in poly(ethylene oxide) (PEO). While PEO chains act as solid solvents for many lithium salts, the limited conductivity at room temperature, low processability, and poor mechanical properties mean that pure PEO/LiX phases are of limited practical use.[4] It is well established that conductivity occurs in the amorphous phase, via a liquidlike motion of cations through the segmental motion of the neighboring chains.[1,5,6] Decreasing T_g appears to be the main path toward obtaining better conductivity. This can be achieved by grafting side chains onto the backbone (comb-shaped systems)[7] or by reducing the likelihood of crystallization by a judicious choice of Li^+ couterion[8,9] or by addition of fine particles to the polymer.[10] The controlled addition of inorganic fillers has been widely studied as a way to increase the processability and stability of the polymer, by an increase in its mechanical modulus. The latest trends in the polymeric electrolyte field are the trapping of lithium salt solutions into a polymer matrix[11,12] so that the processability and mechanical properties of the polymers synergize with liquidlike conductivity.

The sol-gel process appears to be a unique way of designing such materials.[13] Starting from molecular precursors, one can obtain a solid matrix with controlled porosity and filling of the pores. The mixing of organic and inorganic moieties on the molecular scale leads to materials with totally new properties.[14] Moreover, the control of the viscosity from very fluid to very viscous is a useful feature for processing these materials as monoliths or as films of controlled thickness.[14] Such materials called ormocers (organically modified ceramics) or ormosils (organically modified silanes) have been widely developed to possess many useful properties.[15] Electrolytes (so called ormolytes) have already been described and are obtained by the hydrolysis-condensation of amine or benzyl sulfonic modified silanes.[16] Other interesting proposals have been the synthesis of mixed organic-inorganic networks based on TEG/TEOS (tetraethylene glycol/tetraethoxysilane)[17] or glycerol/TiO_2 mixtures[18] in which Li salts are dissolved. Ionic conductivity properties have been measured in these transparent materials.

This paper concerns the study of TEOS/PEG (poly(ethylene glycol)) systems in which large quantities of lithium perchlorate could be dissolved. The structure of these materials is described from the molecular scale (^1H, ^{29}Si and ^{13}C NMR, liquid and solid state) to the structural

* To whom correspondence should be addressed.
† Universität des Saarlandes.
‡ Max-Planck-Institut für Polymerforschung.
§ Present address: Laboratoire de Chimie Structurale Organique (URA CNRS 1384), Université Paris-Sud, Bât. 410, 91405 Orsay, France.
® Abstract published in *Advance ACS Abstracts*, January 1, 1994.

(1) Gray, F. M. *Solid Polymer Electrolytes, Fundamentals and Technological Applications*; VCH Publishers: New York, 1991.
(2) Armand, M. *Adv. Mater.* **1990**, *2*, 278.
(3) Ratner, M. A.; Shriver, D. F. *MRS Bull.* **1989**, 39.
(4) Scrosati, B. *Mater. Sci. Eng.* **1992**, *B12*, 369.
(5) Lightfoot, P.; Mehta, A.; Bruce, P. G. *J. Mater. Chem.* **1992**, *2*, 379.
(6) Boden, N.; Leng, S. A.; Ward, I. M. *Solid State Ionics* **1991**, *45*, 261.
(7) Vincent, C. A. *Electrochemical Science and Technology of Polymers*; Linford, R. G., Ed.; Elsevier Science: London, 1990; Vol. 2, p 47.
(8) Pak, Y. S.; Adamic, K. J.; Greenbaum, S. G. *Solid State Ionics* **1991**, *45*, 277.
(9) Webber, A. *J. Electrochem. Soc.* **1991**, *138*, 2586.
(10) Croce, F.; Scrosati, B. *Chem. Mater.* **1992**, *4*, 1134.
(11) Huq, R.; Farrington, G. C.; Kolsbang, R.; Tonder, P. E. *Solid State Ionics* **1992**, *57*, 277.
(12) Abraham, K. M.; Alamgir, M. *J. Electrochem. Soc.* **1990**, *137*, 1657.
(13) Brinker, C. J. *Sol-Gel Science, the Physics and Chemistry of Sol-Gel Processing*; Academic Press: San Diego, 1989.
(14) Schmidt, H. *Chemistry, Spectroscopy and Applications of Sol-Gel Glasses*; Springer-Verlag, Berlin, 1992; p 117. In *Sol-Gel Technology for Thin Films, Fibers, Preforms, Electronics and Specialty Shapes*; Klein, L. C., Ed.; Noyes: Park Ridge, NJ, 1988.
(15) Schmidt, H. K. *Mater. Res. Symp. Proc.* **1990**, *180*, 961.
(16) Schmidt, H.; Poppal, M.; Rousseau, F.; Poinsignon, C.; Armand, M.; Rousseau, J. Y. *Proc. 2nd Int. Symp. Polym. Electrolytes, Siena, Italy* **1989**, 325.
(17) Ravaine, D.; Seminel, A.; Charbouilot, Y.; Vincens, M. *J. Non-Cryst. Solids* **1986**, *82*, 210.
(18) Judeinstein, P.; Livage, J.; Zarudiansky, A.; Rose, R. *Solid State Ionics* **1988**, *28&30*, 1722.

0897-4756/94/2806-0127$04.50/0

and morphological scale (SAXS, DSC). Complex impedance spectroscopy, in a broad temperature range is used to describe the ionic conductivity properties of such systems. This study emphasizes the relationships between the structure and properties of these materials.

Experimental Section

Materials and Methods. All chemical reagents were commercially available and were used as purchased (Fluka, Aldrich); these included tetraethoxysilane (TEOS), tetraethylene glycol (PEG_4), diethylene glycol (PEG_2), and poly(ethylene glycol) 600 (molecular weight 600, 11–13 ethylene glycol units) (PEG_{12}), hydrochloric acid, and lithium perchlorate ($LiClO_4$). Deionized water was used in all experiments. Infrared spectra were obtained with an IFS25 Bruker Fourier transform spectrometer. The samples were thin films deposited on silicon wafers polished on both sides. Spectra were recorded in the range 4000–400 cm^{-1} with 2-cm^{-1} resolution.

DSC measurements were performed with a Netzsch DSC200 microcalorimeter. Samples (about 20 mg) were cooled to −150 °C, then measurements were performed up to 150 °C (heating rate 20 K/min) under air atmosphere. Glass transition temperatures, T_g, were determined from the midpoint of the experimental curve step.

Liquid-state NMR spectra (^{29}Si and ^{13}C) were obtained on a AC 200 Bruker spectrometer following standard procedures. The chemical shifts were determined within ±0.2 ppm accuracy. Solid-state NMR spectra were obtained at 295 K on a Bruker MSL spectrometer operating at 300 MHz for protons, using magic angle spinning at a rate of 2 kHz. One-dimensional carbon-13 and silicon-29 spectra were recorded with both cross polarization (CP) and single-pulse excitation. Since similar results were obtained, only the cross polarization spectra are discussed here. External tetramethylsilane was used to set the chemical shift scale. As a consequence of the broadening of the peaks, chemical shifts were obtained with uncertanties of ±0.3 and ±1 ppm respectively for ^{13}C and ^{29}Si nuclei. The cross-polarization time was 1 ms in all cases with data acquisition under high-power heteronuclear decoupling (DD) for up to 30 ms. The decoupling field strength was 62 and 45.5 kHz for carbon-13 and silicon-29, respectively. The spectral width was 30 kHz for carbon-13 and 8 kHz for silicon-29. Simple proton spectra were also acquired under magic angle spinning. Two-dimensional proton–carbon and proton–silicon correlation spectra were obtained with the sequence 90° (^1H)–t_1–CP–t_2 (acquire X, DD), using parameters identical to those given for one-dimensional spectra. Data were acquired in t_1 for 16 ms with a spectral width of 5 kHz. This heteronuclear correlation experiment was first demonstrated by Müller and Ernst[19] in a liquid and has been used more recently in solids without major modification to investigate zeolites[20] and polymer blends.[21] In our case, a pure absorption-phase sign discriminated spectrum was obtained by incrementing the phase of the proton 90° pulse in synchronization with the value of t_1.

SAXS was performed on all samples using Cu Kα radiation with a wavelength of λ = 1.54 Å. The SAXS facility utilized a Kratky camera and a linear detector. The samples are small pieces of monoliths of about 1-mm thickness. All the data have been desmeared from the entrance slit geometry (80 μm, 1 cm), and the intensities have been corrected for background scattering and transmission and normalized by the sample thickness, with procedures described elsewhere.[22] Then, the corrected SAXS profiles were plotted in the usual forms (e.g., $I = f(Q)$, where I is the intensity and Q the magnitude of the scattering vector, log $(I) = f(\log Q)$, Zimm, Guinier, etc.) in order to determine the characteristics values of the samples ($Q = 4\pi\lambda^{-1} \sin\theta$, with 2θ scattering angle). The experimental errors are within 0.05 for slope determinations and ±10% for the characteristic dimensions.

Complex impedance spectroscopy was used to determine the electrical properties of the samples. Measurements were performed with a Zahner IM5d apparatus, in the range 0.1 Hz to 1 MHz, with an applied signal amplitude of 50 mV. The sample was a piece of monolith of about 0.2–0.5 mm thickness, with surfaces as flat as possible. The contacts were obtained with plasticized conductive probes (Altoflex, 2 × 2 mm^2) pressed on the sample. The sample holder was placed in a closed thermostated cell, the temperature of which could be controlled in the range −30 to 95 °C (±0.5 °C). Desiccant agents such as P_2O_5 or silicagel were placed in the cell to dry the atmosphere. Prior to the experiment, the aged and dried samples were placed in the measurement cell and conditioned under vacuum at 90 °C for 24 h. The σ values then appear stable and reproducible over the full temperature range.

The materials will be described by the nomenclature $[x]_n[y]$, where x represents the molar ratio [PEG]/[TEOS], n the chain length of the PEG used (n = 2, 4, or 12) and y the ratio [O]/[Li] where oxygens considered are only those of the ether type ($[x]_n$ for materials without Li).

Synthesis. For the sake of clarity, the synthesis of one representative material $[0.5]_4[8]$ is described. TEOS (2.08 g, 10^{-2} mol) was added to 0.97 g of PEG_4 (5×10^{-3} mol) and 0.45 g of water (2.5 10^{-2} mol), under vigorous stirring. The mixture was heated to 60 °C and stirred for 10 min. Afterward, 0.197 g of $LiClO_4$ (1.87×10^{-3} mol) was added and dissolved. Then, 2 μL of concentrated HCl (5×10^{-5} mol) was added, and the blend was mixed to give a monophasic liquid. The liquid was cast in a PTFE vessel, and placed in a 60 °C oven. Gelation of this system occured after 6 days, and the samples were aged 30 days prior to further investigations. Monoliths are then obtained. Further aging of the pellets for 7 days under vacuum (5 Torr) at 100 °C was performed prior to conductivity measurements.

Materials with x = 0.5, 1.8, and 2.3 and y = 2, 4, 8, 15, 30, and 80 have been prepared. The ratio of water was chosen to be $[H_2O]/[Si] = 2.5$.

Transparent materials are obtained for these different compositions. Gel times are shorter for higher amounts of $LiClO_4$ and smaller ratio of organic components. Brittle gels are obtained for smaller ratios of organic in the material. Very soft gummy resins are obtained for higher ratios of PEG_{12}. A density of about 1.5–1.7 was determined by pycnometric measurements, meaning that these materials could be considered as rather compact, without voids.

Results and Discussion

IR Spectroscopy. Infrared spectroscopy clearly shows the development of a network during the gel formation, with broad bands centered around 1170 (ν_{C-O-C}) and 1070 cm^{-1} (ν_{Si-O-C}, $\nu_{Si-O-Si}$). However, their broadness and their overlap with sharp and intense vibrations of the dissolved $LiClO_4$ salt (1147, 1113, and 1089 cm^{-1}) prohibit further investigations of the network formation. A sharp band is observed between 940 and 943 cm^{-1} in $LiClO_4$-doped materials which is characteristic of the symmetric ClO_4^- stretching vibration for solvent-separated ion pairs $[Li(PEG)_nClO_4^-]_s$.[23,24] A broad band in the range 875–885 cm^{-1} could be also observed, characteristic of the metal–oxygen breathing motion, and evidence for the formation of PEO salt and crown ether complexes.[25,26] These results establish the dissolution of the lithium salt in the PEG_n component.

DSC. DSC measurements have been performed on materials $[2]_4$ and $[2]_4[30]$. A glass transition is observed

(19) Müller, L.; Ernst, R. R. *Mol. Phys.* **1979**, *38*, 963.
(20) Vega, A. J. *J. Am. Chem. Soc.* **1986**, *110*, 1049.
(21) Schmidt-Rohr, K.; Clauss, J.; Spiess, H. W. *Macromolecules* **1992**, *25*, 3273.
(22) Strobb, G. R. *Kolloid Z. Z. Polym.* **1972**, *250*, 1039.
(23) Yamanaka, S.; Sarubo, M.; Tadanobu, K.; Hattori, M. *Solid State Ionics* **1992**, *57*, 271.
(24) James, D. W.; Mayes, R. E. *Aust. J. Chem.* **1982**, *35*, 1775.
(25) Papke, B. L.; Ratner, M. A.; Shriver, D. F. *J. Phys. Chem. Solids* **1981**, *42*, 493.
(26) Eschmann, J.; Strasser, J.; Xu, M.; Okamoto, Y.; Eyring, E.; Petrucci, S. *J. Phys. Chem.* **1990**, *94*, 3908.

Scheme 1. ^{13}C NMR Assignments: Hydrolysis of TEOS (Incertitude on Chemical Shift Is ±0.2 ppm)

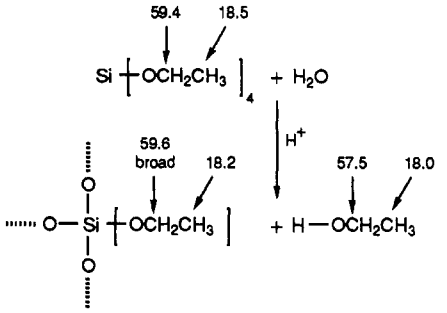

Scheme 2. ^{13}C NMR Assignments: Alcohol-Exchange Reaction (Incertitude on Chemical Shift Is ±0.2 ppm)

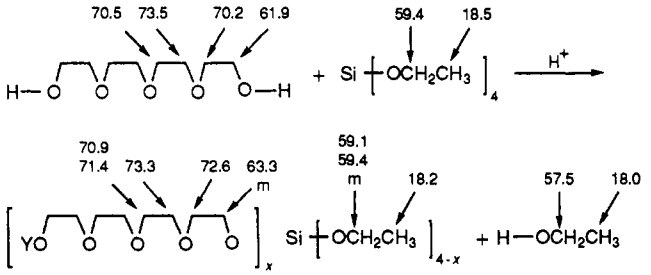

at lower temperature T_g, followed by a cold crystallization associated with a melting peak.[27] No other phenomenon are observed up to 150 °C. T_g are measured at −70 and −50 °C, with the second phenomenon observed around −10 and 5 °C respectively for the compounds without and with Li salt dissolved. Such an increase of transition temperatures with salt doping has been measured in most of polymeric electrolytes, and associated with the decrease of the PEG_n chain mobility.[28,29] The glass transition observed in these materials asserts their polymeric behavior and the restraining of crystallization, as opposed to the individual behavior of PEG_4 molecules of $PEG_4/LiClO_4$ solutions.

NMR Spectroscopy. NMR spectroscopy has been applied to determine the chemistry involved in the formation of these materials in order to clarify their structures.

At least, two reaction steps can occur when TEOS and PEG_n are mixed with water under acid catalysis: an alcohol-interexchange reaction and the hydrolysis of TEOS. These reactions have been studied separately in order to get a tentative assignments of the different ^{13}C peaks, and the data summarized in Scheme 1 and 2.

(*a*) *Hydrolysis Step [1 mol of TEOS + 2.5 mol of H_2O + 0.005 mol of HCl], Figure 1a and Scheme 1.* The main effect is the formation of ethanol (peaks at 57.5 and 18.0 ppm), and the consequent appearance of broad peaks around 15.8 and 59.6 ppm. These latter come from ethoxy groups bonded to silicon atoms. The width of these peaks could be attributed to a large distribution of sites and environments of silicon $(CH_3CH_2OSi(OEt)_{3-x-y}(OH)_{x-y}(OSi)_y)$, because of the grafting of the alkoxy groups to small silica clusters, with low mobilities.

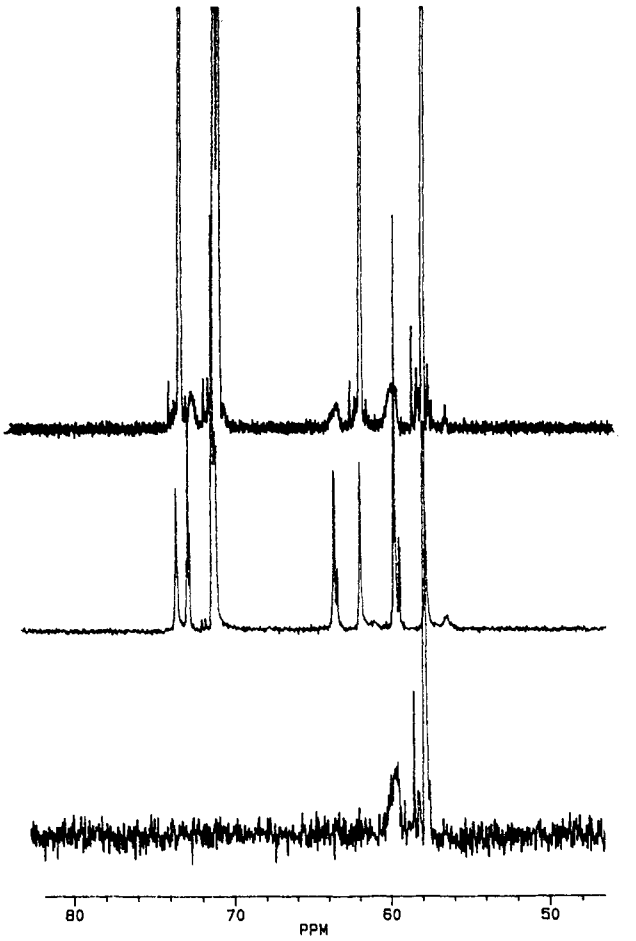

Figure 1. Liquid ^{13}C NMR, (from bottom to top): (a) hydrolysis step, 1 mol of TEOS + 2.5 mol of H_2O + 0.005 mol of HCl; (b) alcohol-exchange step, 1 mol of TEOS + 0.5 mol of PEG_4 + 0.005 mol of HCl; (c) $[0.5]_4$ sample, 24 h after mixing. Only 50 ppm sections are shown.

(*b*) *Alcohol-Interexchange Reaction [1 mol of TEOS + 0.5 mol of PEG_4 + 0.005 mol of HCl], Figure 1b and Scheme 2.* The formation of the four different exchange compounds $(PEG_4)_xSi(OEt)_{4-x}$ $(0 \le x \le 4)$ is suggested by the multiplicity of the peak around 59.3 ppm (CH_3CH_2OSi) and the appearance of four peaks around 63.6 ppm (OCH_2CH_2OSi). Consequently, the decrease of the intensity of the peak at 70.2–70.8 ppm, and the appearance of multiple peaks around 72.6 ppm (OCH_2CH_2OSi) are observed.

While in most previous studies this kind of materials has been studied by the NMR of the metal nuclei,[30] both solid- and liquid-state carbon-13 spectra were found to give useful information. The $[0.5]_4$ blend is considered first as a representative example. Its liquid-state spectrum (Figure 1c), recorded 24 h after mixing shows five intense narrow peaks which corresponds to those of pure PEG_4 and four broad peaks around 15.8, 59.5, 63.2, and 72.5 ppm, corresponding respectively to ethoxy groups bonded to silica clusters and PEG_4 groups bonded to silicon or silica clusters as described earlier.

The solid state CP-MAS spectrum (Figure 2d), recorded after drying, shows seven groups of lines with the small peak at 15 ppm suggesting an almost complete removal

(27) Giles, J. R. M.; Booth, C.; Mobbs, R. H. *6th Riso International Symposium on Metallurgy and Materials Science, Transport-Structure Relations in Fast Ion and Mixed Conductors*; Poulsen, F. W., Hessel, N., Andersen, K., Clausen, S., Skaarup, O., Sørensen, O. T.; Eds.; 1985; p 329.
(28) Spindler, R.; Shriver, D. F. *Macromolecules* **1988**, *21*, 648.
(29) Watanabe, M.; Nagano, S.; Sanui, K.; Ogata, N. *J. Power Sources* **1987**, *20*, 327.
(30) (a) Nabavi, M.; Doeuff, S.; Sanchez, C.; Livage, J. *J. Non-Cryst. Solids* **1990**, *121*, 31. (b) Pouxviel, J. C.; Boilot, J. P.; Beloeil, J. C.; Lallemand, J. Y. *J. Non-Cryst. Solids* **1987**, *89*, 345.

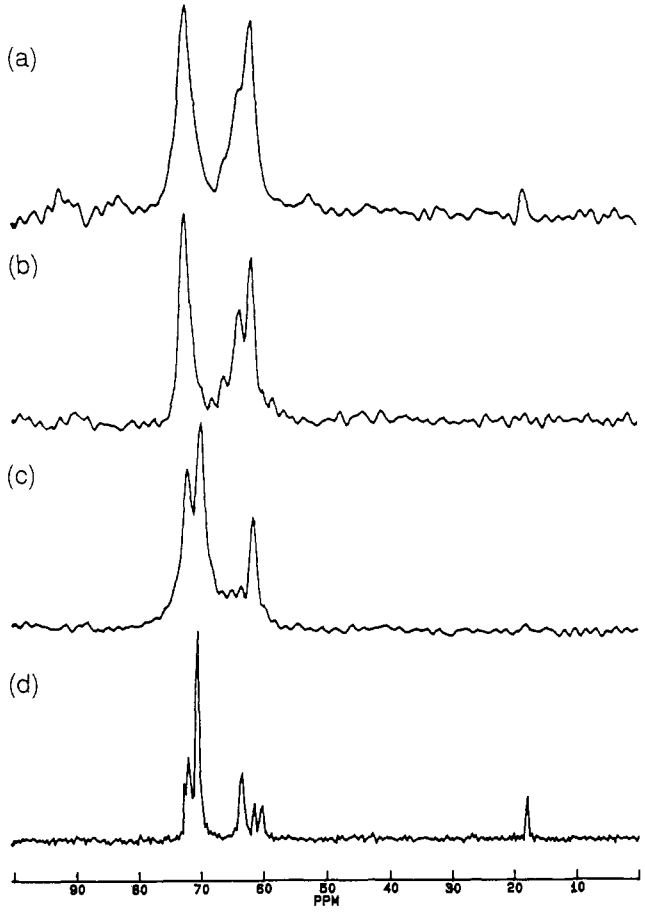

Figure 2. ^{13}C CP-MAS spectra of materials: (a) $[0.5]_2$, (b) $[2]_2$, (c) $[0.5]_4[8]$, (d) $[0.5]_4$, recorded using the parameters given in the text. Only 100 ppm sections are shown.

of the ethoxy groups during gelation and aging of the material. Small variations in the chemical shifts between the liquid and the solid can be explained in terms of conformational changes and hindrance of the chains in the solid state, but broadly speaking, the same groups of lines are obtained. A notable exception is that the 58 ppm line from the pure PEG has completely vanished and the 62 ppm line is much reduced while the other lines in this region of the spectrum are enhanced. The same groups of lines are present in the spectra of all the samples investigated, ($[0.5]_4[8]$, $[0.5]_2$ and $[2.0]_2$) (Figure 2a,c), but in these cases the resolution is reduced because of the greater rigidity of the materials (see below). This prevents any further conclusions about the grafting of the chains.

Simple proton NMR measurements provide a very convenient means of studying the changes in dynamics across the range of materials studied here. Figure 3 shows 5-kHz-wide sections of the spectra for $[0.5]_4$, $[2]_2$, $[0.5]_4$-$[8]$, $[0.5]_4$, $[2]_4$ materials. Those prepared from the higher molecular weight PEG show motionally narrowed spectra with the high PEG ratio materials $[2]_4$ (e) exhibiting resolution of two proton lines separated by less than 1 ppm and a pair of spinning sidebands toward the edges of the sections. Indeed, this material is so mobile that cross polarization fails. Decreasing the PEG_4 ratio (d) leads to broadening indicative of increasing rigidity, while addition of $LiClO_4$ salt (c) results in no major change. The low molecular weight PEG_2 based materials show lines which are broadened still further evidence of their still greater rigidity.

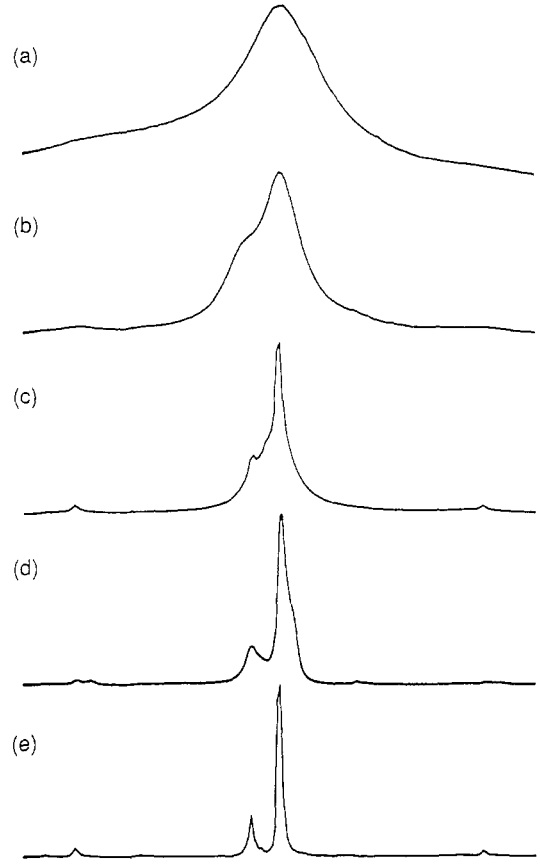

Figure 3. Proton NMR spectra of materials: (a) $[0.5]_2$, (b) $[2]_2$, (c) $[0.5]_4[8]$, (d) $[0.5]_4$, (e) $[2]_4$ recorded using parameters described in the text. The width of the sections shown is 5 kHz. Spinning side bands are observed in (c), (d), and (e).

Perhaps, the most complete picture is provided by the correlation experiments. Figure 4 shows the proton-carbon correlation of the $[0.5]_4$ material, showing in the proton dimension only the 2-kHz region around the largest peak. Several correlations can be observed. First, the large proton signal is associated with the carbon lines at 62, 71, and 73 ppm which are all signals observed for pure PEG_4. In each of these cases, the correlation peak has the form of a doublet of extremely narrow lines, suggesting that these carbon lines are associated with free chains. These nonbound signals dominate for this particular material which explains the overall liquidlike behavior observed in the proton spectra. The signal from the most mobile protons is a doublet because the motional narrowing allows the resolution of the indirect carbon-13–proton spin–spin coupling. Indeed a major component of the cross polarization may be through the indirect coupling for this sample. A value of 170 Hz can be assigned to the splittings observed here which is typical for indirect heteronuclear couplings. The correlation peak at a carbon shift of 71 ppm consists of the doublet sitting on top of a broader component, as can be clearly seen in the contour plot. This might be evidence of a second type of motional behavior associated with the PEG chains bound to the silica, which are somewhat rigid. Similar broader correlations are expected for the carbon peaks at 63.5 and 60.5 ppm although they are not visible above the noise in the two-dimensional spectrum. A different proton signal correlates with the carbon line at 72.5 ppm and again a doublet of narrow lines is observed. Similar results have been obtained for the $[2]_2$ material, although here the lack of sufficient motional narrowing prevents the reso-

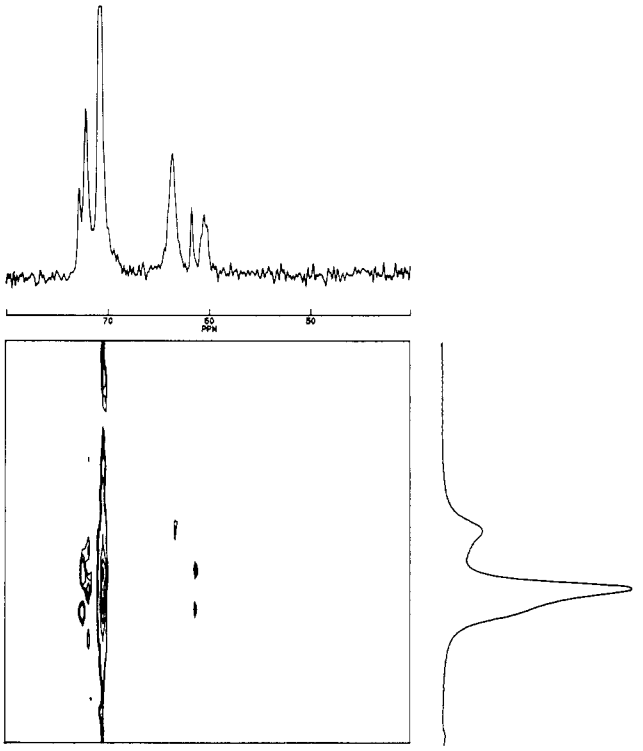

Figure 4. Proton–carbon heteronuclear correlation of material $[0.5]_4$, recorded using the parameters and pulse sequence given in the text. Only positive contours are plotted, there being no negative intensity at these levels. Carbon chemical shifts run along the horizontal axis with proton line shape appearing on the vertical axis. Only a 2-kHz region of the proton spectrum around the narrow peak is shown. Correlations of a doublet form are due to the resolution of ^1H–^{13}C couplings.

lution of heteronuclear couplings. Nevertheless, in all the materials investigated the most mobile component of the proton spectrum is clearly associated with the pure PEG carbon lines, indicating the presence of an organic-rich phase not bound to silicon.

Figure 5 shows the silicon-29 CP-MAS of the $[0.5]_4$ material in which three peaks can be observed around −91, −101, and −110 ppm, characteristic of Q^2, Q^3, and Q^4 environments, respectively. Liquid-state measurements were also made during the formation of the gel; the hydroxylation–condensation occurs so quickly that the same three lines are observed only a few hours after mixing. CP-MAS spectra are not quantitative,[31] the high proportion of Q^2 and Q^3 environments is expected because of the higher proton density close to the surface of the silica particles. Evidence of the structural heterogeneity of the $[0.5]_4$ material is provided by the proton–silicon correlation spectrum. This is also shown in Figure 5 along with the vertically expanded proton spectrum; note that a 5-kHz section is shown here. Both the Q^2 and Q^3 signals are clearly correlated with broad proton signals lying under the main proton line. The increased rigidity suggested by the broader line is evidence of PEG chains bound to silica particles. The lack of a correlation with the narrow proton line is evidence of a spatial separation on the nanometer scale of the silicon-rich and organic rich phases of the material. Such a correlation is expected because of strong proton-proton spin-spin couplings if the protons from the two phases are closer than a few nanometers.

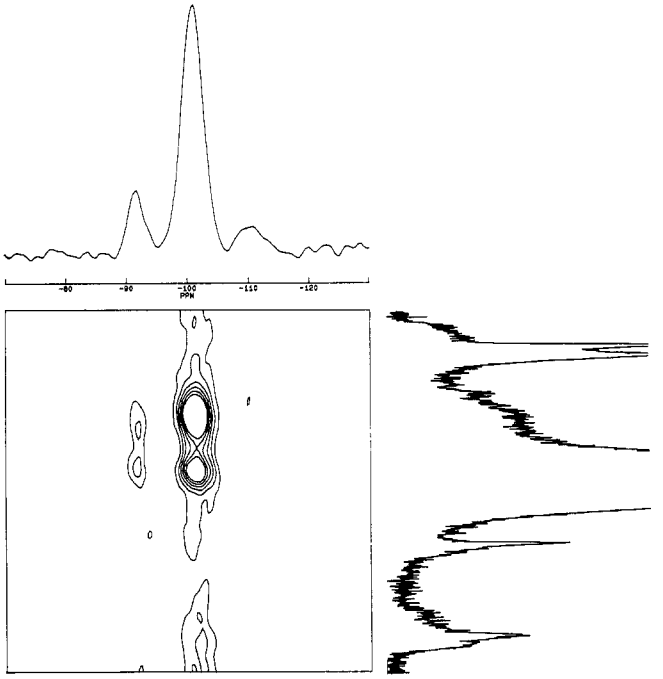

Figure 5. Proton–silicon heteronuclear correlation of material $[0.5]_4$, recorded using the parameters and pulse sequence given in the text. Again, only positive contours are plotted. Here, a 5-kHz region of the proton spectrum is plotted with an expanded vertical scale.

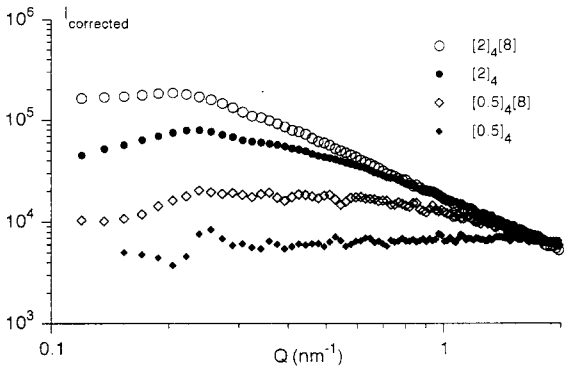

Figure 6. SAXS curve: (a) $[0.5]_4$, (b) $[0.5]_4[8]$, (c) $[2]_4$, (d) $[2]_4[8]$.

SAXS. Figure 6 presents the SAXS curves obtained for different samples, plotted on a log–log graph. These scattering profiles display a very broad interference peak, indicative of a non-highly periodic fluctuation of the electron density within the materials. This result can be explained by a diphasic structure of these compounds, caused by local phase separation between domains rich in silica or organic materials. The maximum position shifts to lower angles with an increase of the content of the organic component. The intensities drastically increase with an increase of the organic component or the dissolution of $LiClO_4$ in the materials.

A model has been proposed to explain similar curves obtained with inorganic–organic network ceramers.[32] The peak position reflects the interdomain spacing, $d = 2\pi/Q$, where d is the interdomain distance and Q the magnitude of the scattering vector. The intensity I scattered by a diphasic system is related to the electron density variation

(31) Devreux, F.; Boilot, J. P.; Chaput, F.; Lecomte, A. *Phys. Rev. A* **1990**, *41*, 6901.

(32) Rodriguez, D. E.; Brennan, A. B.; Betrabet, C.; Wang, B.; Wilkes, G. L. *Chem. Mater.* **1992**, *4*, 1437.

Table 1. Small-Angle X-ray Scattering Results and Interpretations[a]

formula	% vol SiO_2	d (nm) interparticle dist	slope	R_g (nm) Guinier plot	R_g (nm) Zimm plot	R_{calcd} (nm) from d	L (nm) (rod model)	c (nm) (rod model)
$[0.5]_4$	23.6	3.0		0.3	0.5	0.4		
$[0.5]_4[8]$	23.6	24	−1.1	1.1	1.1	3.6	3.8	0.22
$[1]_4$	13.4	3.5		0.8	0.6	0.4		
$[1]_4[8]$	13.4	25	−1.3	1.7	2.1	3.1	6.1	0.4
$[2]_4$	7.1	28	−1.6	2.5	1.9	2.8	8.7	0.6
$[2]_4[8]$	7.1	33	−1.7	3.4	4.7	3.3	11.7	1.1
$[0.5]_{12}[8]$	9.0	26	−1.9	2.2	3.5	2.8	6.5	0.4
$[0.5]_2$	36.1	<1.5				0.2		
$[1]_2$	22.0	2				0.3		
$[2]_2$	12.4	3.1		0.3	0.4	0.4		

[a] Silica volume ratio (% vol SiO_2), interparticle distance (d), slope of the curve, Guinier radius (R_g) determined by Guinier and Zimm plot, theoretical radius (R) determined in regard to the experimental d value, length (L), and diameter (c) of the particles considering a rod-size shape as a function of the material composition. The experimental errors are within 0.05 for slope determinations and ±10% for characteristic dimensions.

$\Delta\rho$ by the relation $I \propto (\Delta\rho)^2 N$, where N is the number of scatterers. Then, the maximum intensity gives information on the number of particles, and the slope (or the curvature) of the profile reflects the sharpness of the boundaries between phases, as it could also be stated from the fractal theory.[33] Lower slopes are representative of more diffuse scatterers or/and less compact surfaces. Moreover, an estimate of the size of the particle could be established from Guinier or Zimm plots, following usual analysis.[34]

Table 1 summarizes the results obtained from the analysis of the different curves. In the set of samples $[x]_4$, the effect of x on the material morphology could be followed. Compounds with higher silica ratio flat curves with a low intensity. Results from calculations lead to a radius of gyration R_g of about 0.4 nm and an interparticle distance of about 3 nm. This means a great homogeneity in the material on the SAXS scale. An increase of the size of the particles and of the interparticle distances is observed with a decrease of the silica ratio. A slope of −1.6 could be measured for the $[2]_4$ compound meaning that the silica particles have a random shape, a very low surface density, and an anisotropic frame. Such dimensions could also correspond to swollen polymers[35] or fractal objects.[33]

The radius of the particles and the interparticle distances strongly increase, upon addition of $LiClO_4$ in the different $[x]_4$ samples. The intensity of the signal increases, meaning that the number of scatterers increases and the diphasic character of the material gets more pronounced. Silica particles are better defined in the presence of $LiClO_4$. In fact, the structural effect can be assumed to be even larger as measured from the intensity of the curves, since $LiClO_4$ dissolved in the organic phase should decrease the electron contrast $\Delta\rho$ between the two phases. Nonetheless, the moderate change of the slope may indicate that the particle shape is hardly changed. These particles could be treated as anisotropic rods[36] or still be considered shaped more like swollen polymer of increased size. The calculation for the rod model is reported in Table 1.

These results point out the effect of the addition of inorganic salt on the morphology of sol–gel materials. The size of the SiO_2 particles is evidently greatly affected. This can be only explained by some change in the involved chemistry.[37] The effect of variation of the chain length of the PEG_n polymer appears to be moderate. It acts mainly through the change of the SiO_2 ratio, with the subsequent change of the interparticle distance and particle size.

The calculated inter- and intradimensions are compared with those obtained from a theoretical calculation. In this model, it is assumed that silica particles form compact spheres of radius R. If d is the distance between two of these particles, the following relation can be verified: $R = (\%\ \mathrm{vol}_{[SiO_2]} \cdot 3/8\pi)^{1/3} d/2$. The values of R calculated from this relation on the basis of the experimental d values are also reported in Table 1. The slight discrepancies of those values with the experimental ones can be explained by the nonregular polymeric or anisotropic structure of SiO_2 particles. However, the results of these calculations confirm the initial hypothesis used for the interpretation of the SAXS curves.

Conductivity Measurements. As usually observed for ionic conductors, electrical impedance, plotted in the complex plane exhibits an arc of circle at high frequencies that corresponds to the bulk conductivity of the sample, followed by a vertical linear variation at lower frequencies due to the interface between the gel and the blocking electrodes.[38] The intercept of the arc of circle with the real axis gives the ohmic resistance from which conductivity σ can be deduced.

Figure 7a presents the changes of room temperature conductivity, σ_{RT}, measured at 20 ± 1 °C, with composition variations. Values of conductivity between $10^{-8}\ \Omega^{-1}\ cm^{-1}$ and $6 \times 10^{-5}\ \Omega^{-1}\ cm^{-1}$ are measured. These values are large enough in regard to the conductivity measured for the pure matrix (TEOS/TEG/H_2O/HCl with the same ratios; $<10^{-10}\ \Omega^{-1}\ cm^{-1}$) to assume that the conductivity occurs mostly from the dissolved salts. Nonetheless, a contribution from a mixed ion conductivity effect cannot be excluded. The conductivity values reported in graphs and tables correspond to anhydrous materials after vacuum and heat treatment. The decrease of conductivity from aged materials to deep-dried materials is more than 3 decades. An huge increase of conductivity with Li^+ concentration is observed for both PEG_2 and PEG_4 systems. Nonetheless, this behavior is in contrast with

(33) Schaeffer, D. W.; Keefer, K. D. *Mater. Res. Soc. Symp. Proc.* **1984**, *34*, 1.
(34) Glatter, O.; Kratky, O. *Small Angle X-Ray Scattering*; Academic Press: New York, 1982.
(35) Flory, P. J. *Principles of Polymer Chemistry*; Cornell University Press: Ithaca, NY, 1953.
(36) Jutson, J. A.; Richardson, R. M.; Jones, S. L.; Norman, C. *Mater. Res. Soc. Symp. Proc.* **1990**, *180*, 123.
(37) Henry, M.; Jolivet, J. P.; Livage, J. *Chemistry, Spectroscopy and Applications of Sol-Gel Glasses*; Springer-Verlag: Berlin, 1992; p 117.
(38) Linford, R. G. *Electrochemical Science and Technology of Polymers*; Linford, R. G., Ed.; Elsevier Science: London, 1990; Vol. 2, p 281.

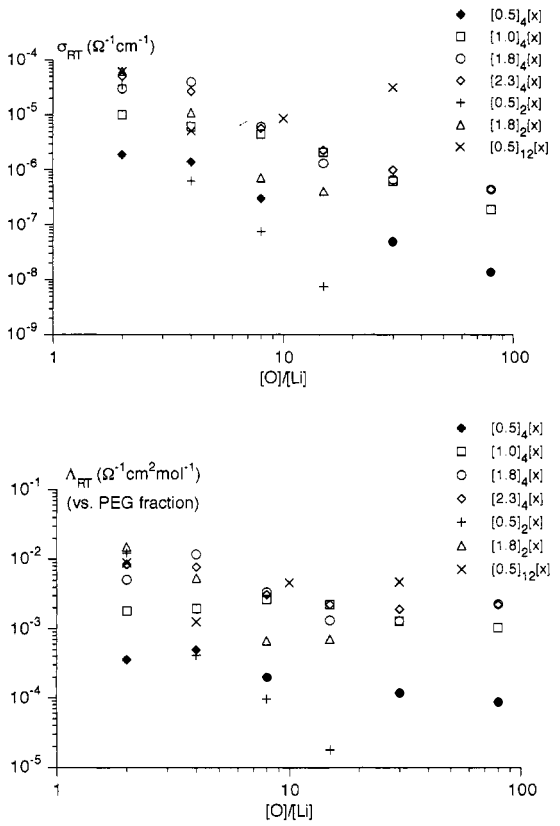

Figure 7. Ionic conductivity measured at room temperature (20 ± 1 °C) as a function of [O]/[Li]: (a) σ_{RT}; (b) Λ_{RT} (in regard to the polymeric PEG_n phase).

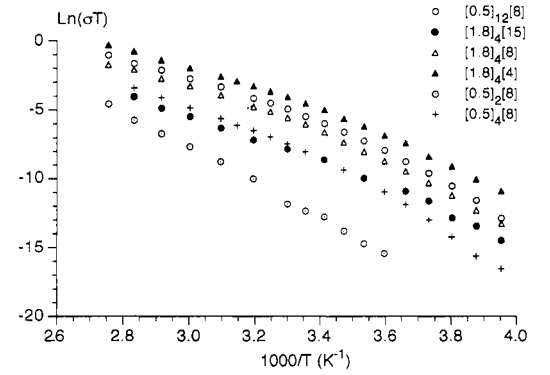

Figure 8. Temperature dependance of ionic conductivity for different materials.

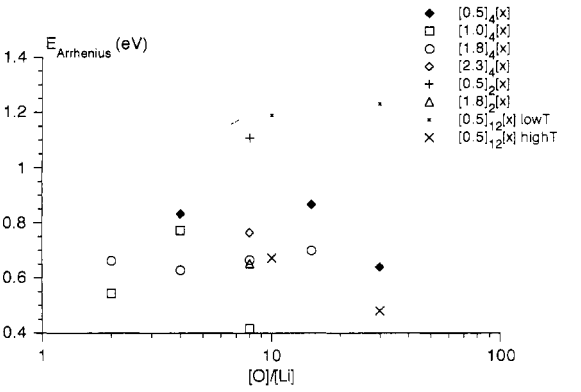

Figure 9. Influence of composition on activation energy E_a.

those observed for most of the polymeric systems in which a maximum conductivity is observed for [O/Li] around 8.[29,39] One of the current interpretations of this phenomenon has been provided recently by McCallum and Vincent.[40] They attributed the increase in conductivity with increasing the salt concentration to long-range coulomb interactions (also referred as coulomb screening). The decreasing observed after the maximum is a consequence of the immobilization of the polymer chains by interactions with the ions. Spectroscopic investigations suggest a diphasic structure for the materials, where the lithium salts can be only dissolved in the polymeric phase (PEG_n). Then, the variation of the molar conductivity Λ_{RT} determined in respect to the polymeric phase presented on Figure 7b is more informative. Most of PEG_4 (and to a less extent also PEG_{12}) based materials present the expected maximum Λ_{RT} values for [O]/[Li] around 4. Nonetheless, the materials based on PEG_2 present a net increase of Λ_{RT} for the full range of data.

Figure 8 presents the variation of the conductivity with temperature for characteristic samples. For all samples, discrepancies with pure Arrhenius [$\sigma T = \sigma_0 \exp(-E_a/RT)$] or free volume (VTF) [$\sigma T^{1/2} = \sigma_0 \exp(-E_a/R(T - T_0))$] models are observed.[1,3]

Mostly, these plots reveal two slopes, with an intercept around −5/0, 3/10, and 15/20 °C, respectively, for PEG_2-, PEG_4-, and PEG_{12}-based systems. The corresponding activation energy E_a are around 0.5/0.8 and 1.2/1.4 eV respectively for higher and lower temperature processes. Such behavior has also been observed in some polymer[27] or composite electrolytes[41] and interpreted as partial crystallization and phase separation of the material below a critical temperature. Moreover, the range of magnitude of these critical temperatures is not so far from the melting point of pure PEG_2 (−10.5 °C), PEG_4 (−6.2 °C) or softening point of PEG_{12} (17–22 °C), and the observed variations could be explained by the well-known effect of salt concentration at the melting and glass points of polymers.[28] Figure 9 presents the variation of the Arrhenius activation energy E_a of the high-temperature process for different systems. Pseudoactivation energies from 7×10^{-2} to 12×10^{-2} eV are calculated using the VTF model (with T_0 around 200 K). These measured values are higher than reported values for polymeric[2] or composite electrolytes[18,42] but similar to those observed for systems in which big anions are complexed.[8] The highest values of E_a are observed for [O]/[Li] around 10, as has also been observed in liquid polymeric electrolyte.[43] Hindrance of the movement of the polymer chains from the small silica cluster could explain such behavior. This could be confirmed by the $[0.5]_2[x]$ system presenting typical features as very high E_a (>1.1 eV), and a great increase of conductivity with increase of x. Moreover, this should be related to the specific behavior of this system observed on the basis of NMR spectroscopy, presenting a real strong solid-state behavior.

(39) Tsuchida, E.; Shigehara, K. *Mol. Cryst. Liq. Cryst.* **1984**, *106*, 361.
(40) McCallum, J. R.; Vincent, C. A. *Polymer Electrolyte Reviews*; McCallum, J. R., Vincent, C. A., Eds.; Elsevier: London, 1987; p 23.
(41) Huang, X.; Chen, L.; Huang, H.; Xue, R.; Ma, Y.; Fang, S.; Li, Y.; Jiang, Y. *Solid State Ionics* **1992**, *51*, 69.
(42) Charbouillot, Y.; Ravaine, D.; Armand, M.; Poinsignon, C. *J. Non-Cryst. Solids* **1988**, *103*, 325.
(43) Albinsson, I.; Mellander, B. E.; Stevens, J. R. *J. Chem. Phys.* **1992**, *96*, 681.

Conclusion

Organic–inorganic materials showing interesting ionic conductivities were prepared by the sol–gel process. The chemical synthesis of such materials is the key to the control and optimization of the processing and properties. However, the first guide to enhancement of these is the study of structure–property relationships. The multifold framework of such materials requires multitechnique investigation to complete their description.

$TEOS/PEG_n/H_2O/LiClO_4$ mixtures lead to transparent monoliths and films with conductivities up to $5 \times 10^{-5}\ \Omega^{-1}\ cm^{-1}$. Their thermal stability has been checked in the −25/+95 °C range, and the mean conductivity activation energy was measured in the range 0.5/0.9 eV depending on the composition of the blend. However, the phenomenological approach of the conductivity measurements establish some singularities in the behavior of these materials, in regard to the classical VTF model for polymeric electrolyte.

The whole set of data indicate the real diphasic structures for these materials. SAXS shows that low-density SiO_2 clusters (fractallike) are formed. Their size and shape depend the material composition. The PEG_n phase dissolves the $LiClO_4$ salts. However, the interpenetration of these two phases in the nanometer range could explain the polymeric behavior observed with the DSC measurements. NMR measurements clear up the structure on the molecular scale. PEG_n chains partially react with the silicon atoms to produce silica clusters with comb like grafted chains. Most of the PEG_n molecules (n = 4 and 12) are simply entrapped in the network. This gives the dynamic behavior of a liquid system, observed through the NMR experiments. The organic phase appears as a very mobile system, leading to the liquid features measured by the ionic conductivities. Nonetheless, the interpenetration of these two phase at a molecular level, leads also to some collective behavior usually encountered in polymeric systems, such as a glass transition. Moreover, this excellent dispersion and mixing of phases leads to electrolytes with optical transparency and better stability and mechanical behavior than for most pure polymeric systems. These materials combine two goals required in the field of polymeric electrolytes by the simultaneous presence of plasticizers (TEG molecules) and fillers (SiO_2 particles).

Acknowledgment. This work was supported by the Minister for Research and Culture of the State of Saarland. P.J. gratefully acknowledges support of this work by Alexander Von Humboldt-Stiftung. The authors appreciate the assistance of M. Bach for his help in obtaining SAXS curves, and Dr. N. Merl for helpful discussions. J.T. is grateful to Prof. H. W. Spiess in whose laboratory the NMR work was carried out.